Shock propagation in Galilean and special relativity

Robert BLAGA, Victor E. AMBRUŞ

West University of Timisoara, Faculty of Physics, Romania

robert.blaga@e-uvt.ro



Abstract

We employ quadrature-based lattice Boltzmann models for the study of the propagation of fluids in setups containing shocks. We show that our models can accurately capture the features of the flow for all degrees of rarefaction, from the hydrodynamic regime to the free-streaming regime. The decrease of the adiabatic index from 5/3 to 4/3, as we pass from the non-relativistic to the ultrarelativistic limit, induces qualitative changes in the hydrodynamic fields. We highlight key similarities and differences between these regimes.

Introduction

The relativisite Boltzmann equation, with the Anderson-Witting collision term:

 $p^{\mu} \frac{\partial f}{\partial x^{\mu}} = \frac{p^{\mu} u_{\mu}}{\tau} (f - f^{\text{(eq)}}), \tag{1}$

where p^{μ} is the particle 4-momentum, obeying the mass-shell condition $p^2=\eta_{\mu\nu}p^{\mu}p^{\nu}=0$. The Maxwell-Jüttner equlibrium distribution functions:

 $f^{\text{(eq)}} = \frac{n}{8\pi T^3} \exp\left(\frac{p^{\mu} u_{\mu}}{T}\right) \tag{2}$

The macroscopic fields are obtained as moments of the distribution function:

$$\begin{pmatrix}
N^{\mu} \\
T^{\mu\nu} \\
\vdots \\
T^{\mu...\omega}
\end{pmatrix} = \int_{0}^{\infty} dp \, p \int_{-1}^{1} d\xi \int_{0}^{2\pi} d\varphi \, f \begin{pmatrix} p^{\mu} \\
p^{\mu}p^{\nu} \\
\vdots \\
p^{\mu}...p^{\omega} \end{pmatrix}, \quad (3)$$

where $\xi = \cos \theta$. The energy-momentum tensor of an ultra-relativistic fluid is given by:

$$T^{\mu\nu} = (E+P)u^{\mu}u^{\nu} + P\eta^{\mu\nu} + q^{\mu}u^{\nu} + q^{\nu}u^{\mu} + \Pi^{\mu\nu}, \tag{4}$$

where E and P represents the energy and pressure, q^{μ} the heat-flux, while $\Pi^{\mu\nu}$ is the shear-stress tensor.

Relativistic Lattice Boltzmann model

The road to building our lattice Boltzmann models [2] has two steps:

• projecting $f^{\text{(eq)}}$ onto an orthogonal set of polynomials

 $f^{\text{(eq)}}(t, \vec{x}, \vec{p}) = \frac{e^{-p/T_0}}{T_0^3} \sum_{\ell=0}^{N_L} \sum_{s=0}^{N_\Omega} a_{\ell,s}^{\text{(eq)}}(\vec{x}, t) P_s(\cos \gamma_u) L_{\ell}^{(2)}(p/T_0) \quad (5)$

The series is truncated at the finite values N_L, N_Ω

• introducing the Gauss quadrature relations $(v^{\alpha} = p^{\alpha}/p)$:

$$N^{\hat{\alpha}} = \int_{0}^{\infty} dp \, p^{2} \int_{-1}^{1} d\xi \int_{0}^{2\pi} d\varphi \, f \, v^{\hat{\alpha}} = \sum_{a=1}^{Q_{L}} \sum_{b=1}^{Q_{\xi}} \sum_{c=1}^{Q_{\varphi}} f_{abc} \, v_{bc}^{\hat{\alpha}}, \qquad (6)$$

$$T^{\hat{\alpha}\hat{\beta}} = \int_{0}^{\infty} dp \, p^{3} \int_{-1}^{1} d\xi \int_{0}^{2\pi} d\varphi \, f \, v^{\hat{\alpha}} v^{\hat{\beta}} = \sum_{a=1}^{Q_{L}} \sum_{b=1}^{Q_{\xi}} \sum_{c=1}^{Q_{\varphi}} f_{abc} \, p_{a} v_{bc}^{\hat{\alpha}} v_{bc}^{\hat{\beta}}, \qquad (6)$$

$$f_{abc} = \frac{2\pi w_{a}^{L} w_{b}^{\xi}}{Q_{\varphi} e^{-p_{a}/T_{0}}/T_{0}^{3}} \, f(p_{a}, \xi_{b}, \varphi_{c}).$$

This gives us a prescription for choosing the discrete set of momenta. If the value of Q_L, Q_ξ, Q_ϕ is taken large enough, depending on the order of the integrated polynomial, the above sums are exact.

Numerical results

Setup:Riemann problem

We initialize the system with the state [6]:

$$(P, n, \beta) = \begin{cases} (P_{\rm L} = 1, & n_{\rm L} = 0.1, & \beta_{\rm L} = 0), & \text{if } z < 0, \\ (P_{\rm R} = 0.1, n_{\rm R} = 0.125, \beta_{\rm R} = 0), & \text{if } z > 0. \end{cases}$$
(7)

Inviscid regime $(\tau \to 0)$

The flow develops a rarefaction wave moving into the denser region (left), and a shock-wave and contact discontinuity moving towards the more tenuous region (right). As we decrease the relaxation time, the simulated profiles converge towards the analytic solution obtained from ideal hydrodynamics ($\tau \to 0$).

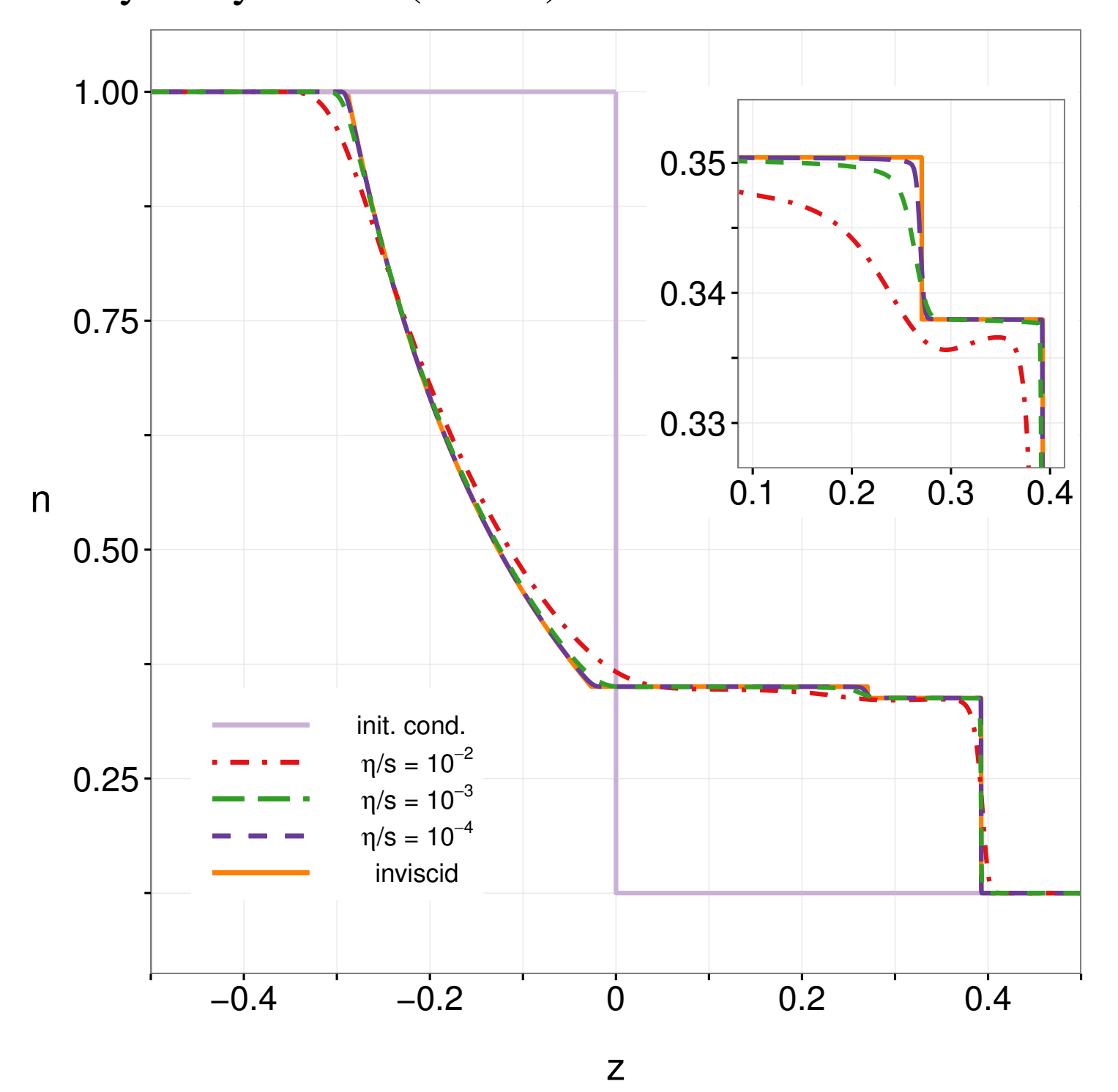


Figure 1: Density profile of the fluid at time t=0.4, at various relaxation times. The quadratures orders are set to $Q_L=2, Q_\phi=1, Q_\xi=4$. The spatial lattice has $L_z=10000$ nodes, while the time step is taken to be $\delta t=5\times 10^{-6}$.

In five-field theory, the non-equilibrium quantities (dynamic pressure, heat-flux and shear-stress) are proportional to the gradients of the macroscopic fields. If the flow contains shocks, the heat flux, for example, is related to the gradients of the pressure and temperature as follows:

$$q^{\mu} = \frac{\lambda T}{4} \Delta^{\mu\nu} \partial_{\nu} \ln \left(\frac{P}{T^4} \right), \qquad \Delta^{\mu\nu} = \eta^{\mu\nu} + u^{\mu} u^{\nu}$$
 (8)

In our case, as the system is homogeneous along the x and y axis, the heat-flux has only one degree of freedom: $q^{\mu} = q(\beta, 0, 0, 1)$.

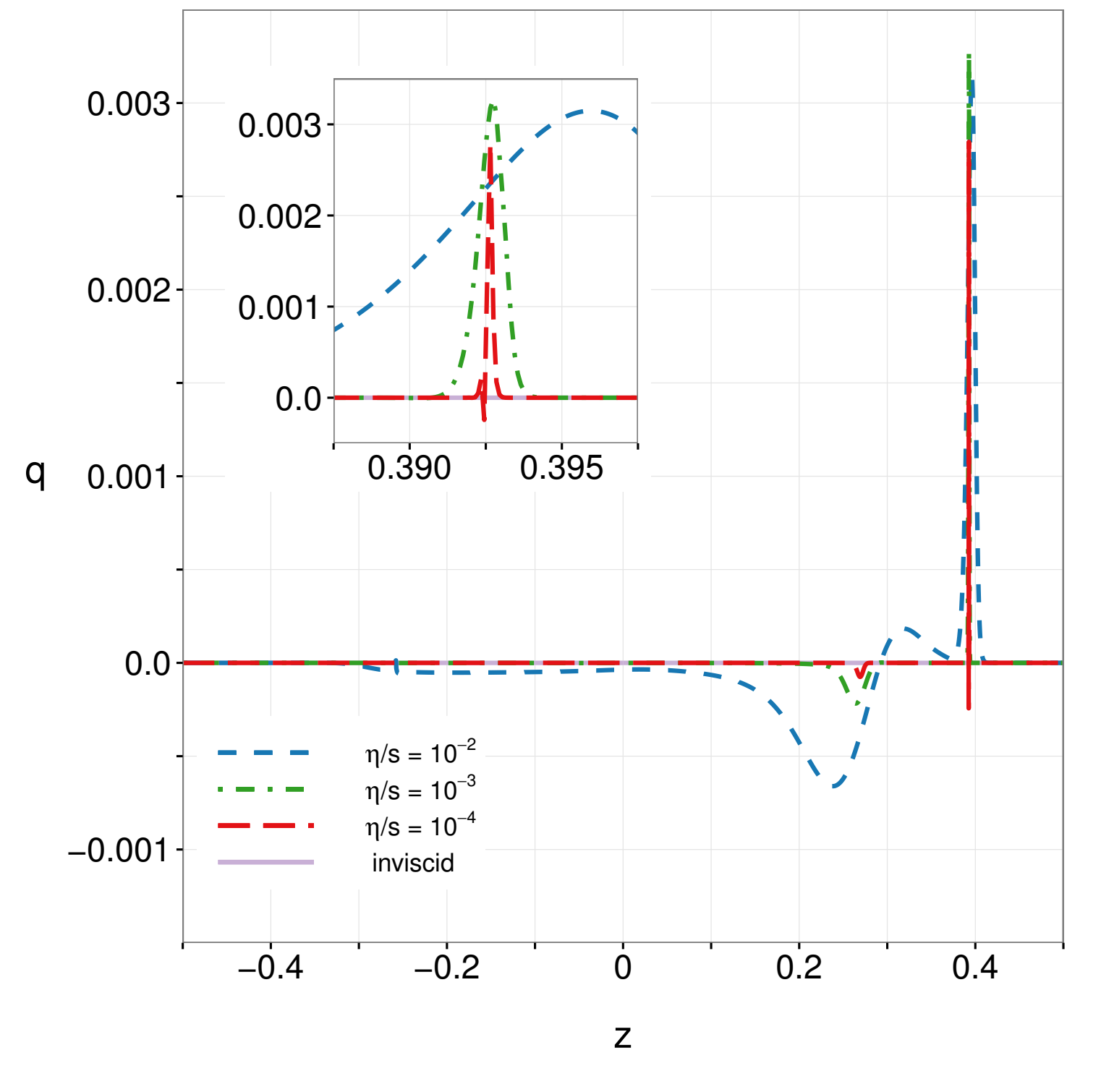


Figure 2: Magnitude of the heat-flux. As the relaxation time is decreased the non-equilibrium quantities are reduced to narrow spikes around the shock front and contact discontinuity.

The parameter λ is the heat conductivity, and in the ultrarelativistic limit can be seen to take the following form: $\lambda = \frac{4P\tau}{3T}$, when obtained through the Chapman-Enskog method. If instead one would use Grad's method, the result would be $\lambda = \frac{4P\tau}{5T}$. It is still an open question which of the above is the correct form, however there have been a number of recent results which suggest that the Chapman-Enskog method gives the correct results [1, 4, 5]. This can be seen also here, if we integrate the heat-flux over a small area around the contact discontinuity:

$$\int_{z_{\rm C}-\delta z}^{z_{\rm C}+\delta z} q \, dz = \frac{1}{8} (\lambda_{\rm I} T_{\rm I} + \lambda_{\rm II} T_{\rm II}) \ln \left(\frac{P_{\rm II}}{T_{\rm II}^4} \frac{T_{\rm I}^4}{P_{\rm I}} \right). \tag{9}$$

One can do similarly for the heat-flux and the shear pressure around the shock front. The results are shown in Fig.3.

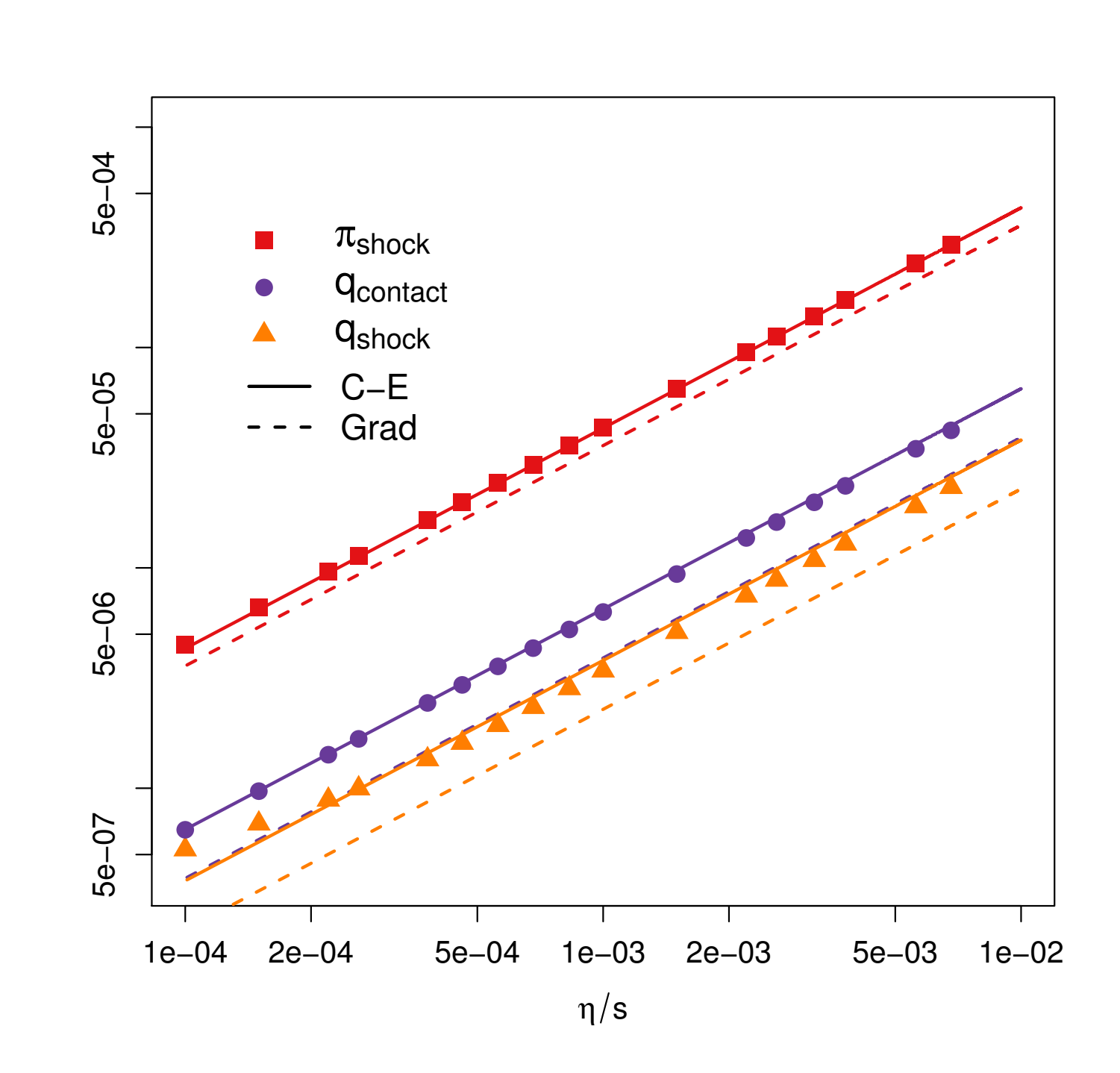


Figure 3: The absolute values of the heat-flux and shear pressure, integrated over a small area around the contact discontinuity and shock front. The shear pressure around the contact discontinuity vanishes, since it is proportional to the velocity gradient, which in turn vanishes because the velocity is constant there.

Ballistic regime $(au o \infty)$

In this regime the fluid constituents are streamed freely and the flow does not develop any distinguishable features. The staircase-like profile is due to the fact that the populations corresponding to each quadrature value are evolved independently. A large number of velocities is thus required in order to obtain a smooth profile.

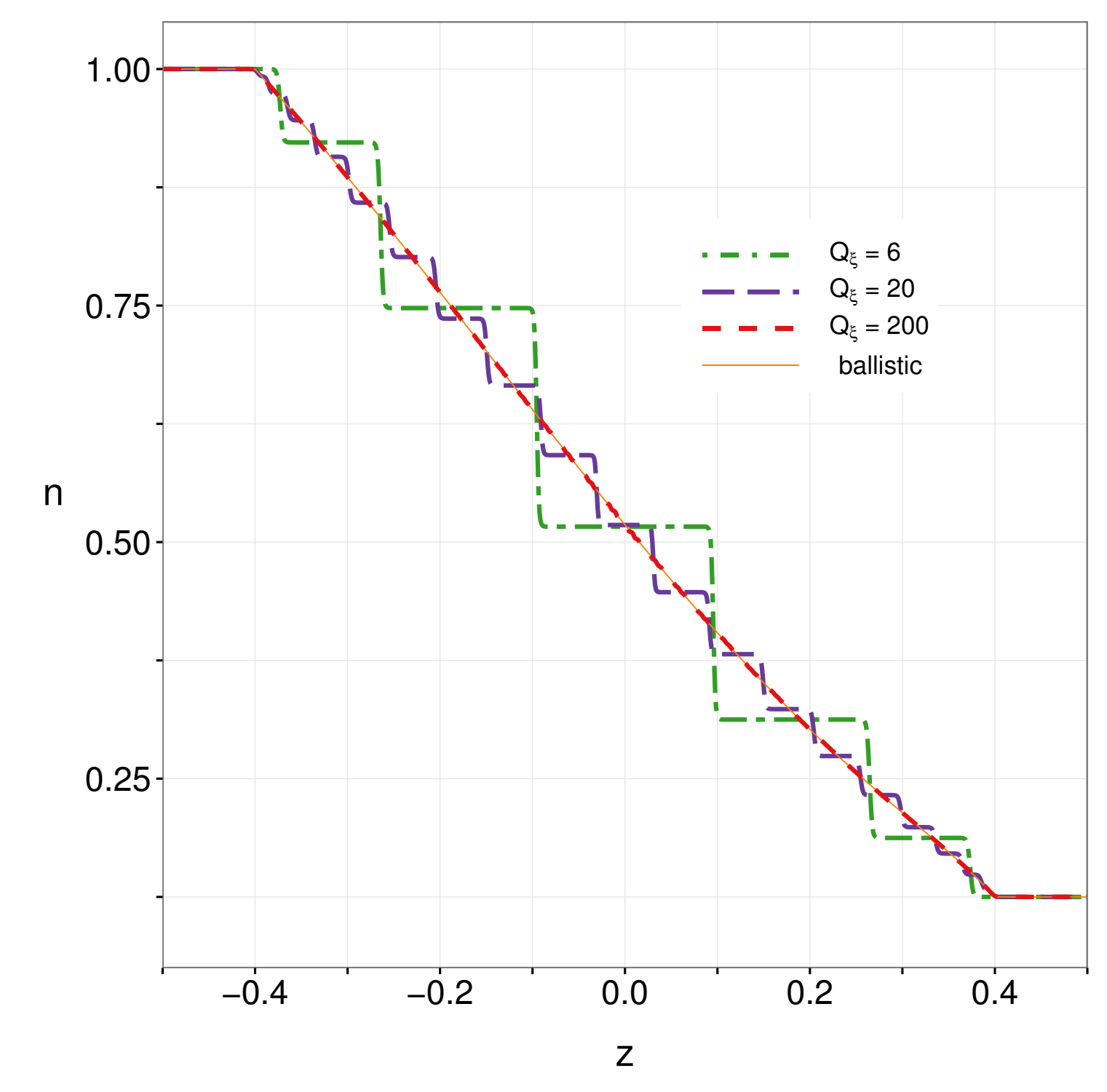


Figure 4: Density profile of the fluid in the ballistic regime, for increasing values of the polar quadrature. The spatial lattice is taken to be $\delta_z = 10^{-4}$, while the time step is $\delta t = 5 \times 10^{-4}$.

Viscous regime

At intermediate relaxation times dissipative effects become relevant. The relaxation time is directly proportional to the transport coefficients and with the shear viscosity (η) in particular:

$$\tau = \frac{\eta}{s} \frac{5}{T} \left(1 - \frac{\ln \lambda}{4} \right),\tag{10}$$

where s the entropy density and $\lambda = n/T^3$ the fugacity. We compare our results with those reported in Ref.[3], which where obtained using a microscopic transport model (BAMPS).

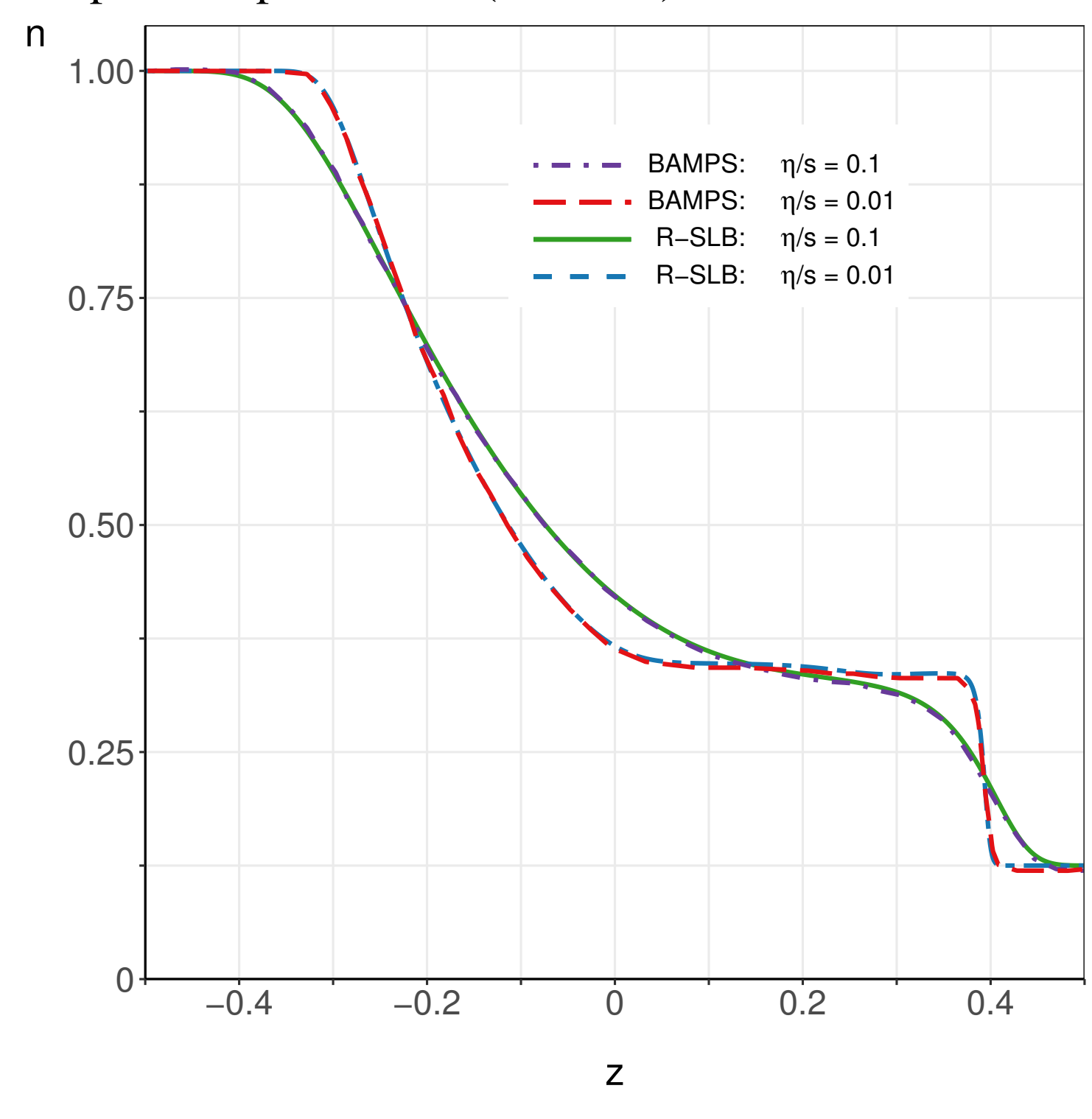


Figure 5: Density profile of the fluid in the intermediate regime. The simulations are performed by keeping η/s constant.

Newtonian vs. ultra-relativistic fluid

There is a qualitative change as we pass from the non-relatvistic regime, with adiabatic index $\gamma = 5/3$, to the ultrarelativistic regime, where the fluid has $\gamma = 4/3$. As a consequence, we can see a significant difference between the macroscopic profiles of the fluid, when comparing the simulation results in the two cases, given the same initial conditions, as can be seen from Fig.6. In particular, note the different values of the plateaus, even though the peak velocity in the relativistic flow is $\beta \simeq 0.46$.

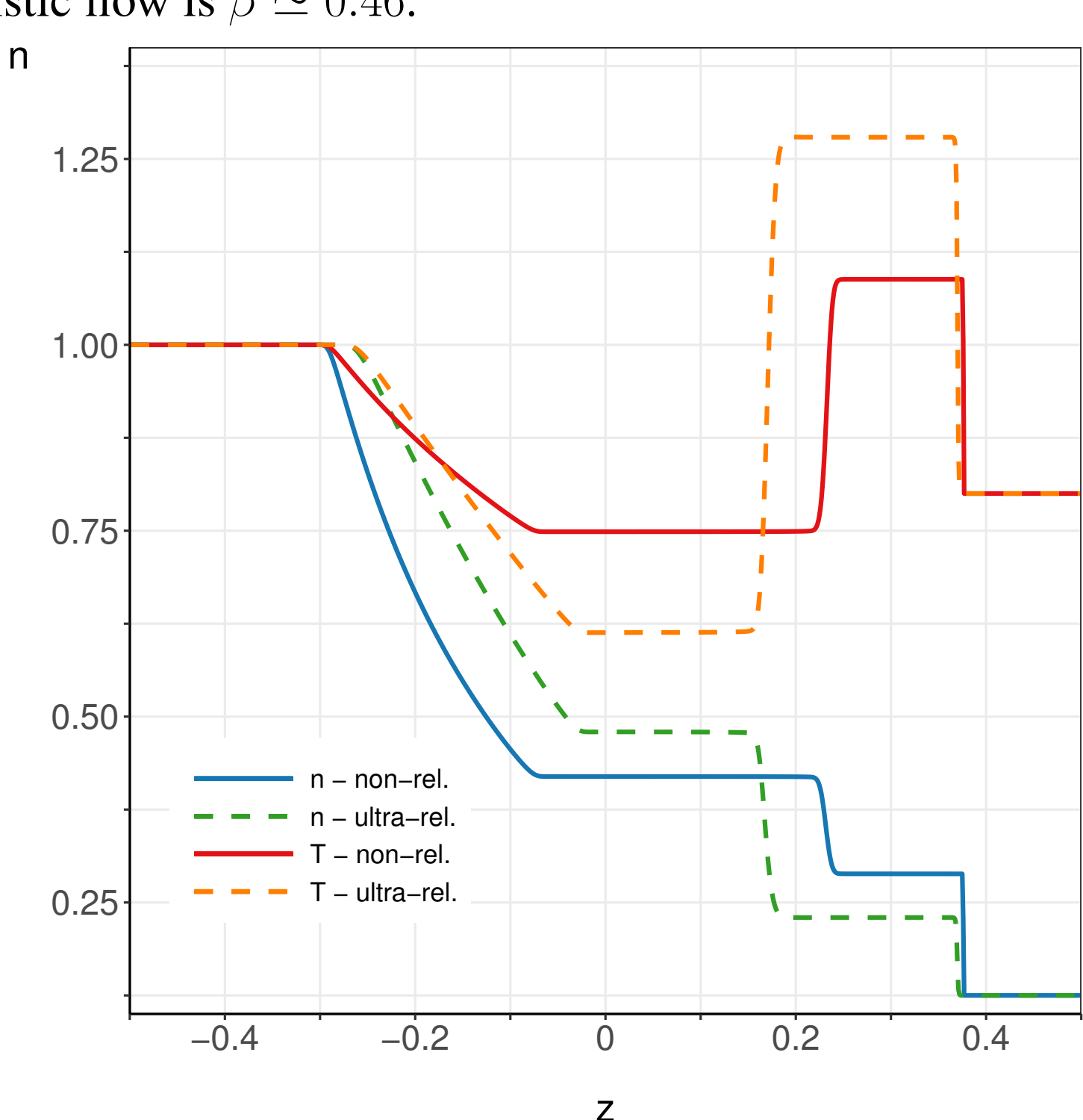


Figure 6: Density and temperature profiles for a non-relativistic and an ultra-relativistic fluid. Both simulations are initialized with the state (7).

Conclusions

The lattice Boltzmann models developed here can be used as a reliable tool for simulating relativistic flows containing shocks. Possible areas for future applications include the physics of quark-gluon plasma and the astrophysical arena.

Acknowledgement

This work was supported by a grant from the Romanian National Authority for Scientific Research and Innovation, CNCS-UEFISCDI, project number PN-II-RU-TE-2014-4-2910.

References

[1] V. E. Ambrus. arXiv:1706.05310, 2017.

[2] R. Blaga and V. E. Ambrus. arXiv:1612.01287, 2016.

[3] I. Bouras, E. Molnar, H. Niemi, Z. Xu, A. El, O. Fochler, C. Greiner, and D. Rischke. *Phys. Rev. Lett.*, **103**, 2009.

[4] A. Gabbana, M. Mendoza, S. Succi, and R. Tripiccione. *arXiv:1704.02523*, 2017.

[5] A. Jaiswal. *Phys. Rev. C*, **87**, 2013.

[6] L. Rezzolla and O. Zanotti. *Relativistic hydrodynamics*. Oxford University Press, 2013.